

Emergence of interparticle friction in attractive colloidal matter

Berend van der Meer^{1,2}, Taiki Yanagishima^{2,3}, Roel P. A. Dullens^{1,2}

¹*Institute for Molecules and Materials, Radboud University,
Heyendaalseweg 135, 6525 AJ, Nijmegen, The Netherlands*

²*Department of Chemistry, Physical and Theoretical Chemistry Laboratory,
University of Oxford, South Parks Road, Oxford OX1 3QZ, United Kingdom and*

³*Department of Physics, Graduate School of Science, Kyoto University,
Kitashirakawa Oiwake-cho, Sakyo-ku, Kyoto, 606-8502, Japan*

(Dated: September 27, 2022)

Interparticle friction plays a governing role in the mechanics of particulate materials [1–16]. However, virtually all experimental studies to date rely on measuring macroscopic responses [1, 2, 8–15], and as such it remains largely unknown how frictional effects emerge at the microscopic level. This is particularly challenging in systems subject to thermal fluctuations due to the transient nature of interparticle contacts. Here, we directly relate particle-level frictional arrest to local coordination in an attractive colloidal model system. We reveal that the orientational dynamics of particles slows down exponentially with increasing coordination number due to the emergence of frictional interactions, the strength of which can be tuned simply by varying the attraction strength. Using a simple computer simulation model, we uncover how the interparticle interactions govern the formation of frictional contacts between particles. Our results establish quantitative relations between friction, coordination and interparticle interactions. This is a key step towards using interparticle friction to tune the mechanical properties of particulate materials.

Over the last decade, a consensus has emerged that interparticle friction plays a crucial role in setting the mechanical and flow properties of concentrated suspensions of particles [1–16]. Despite its importance for tuning the material properties of colloidal systems [6–18], interparticle friction constitutes a largely unexplored control parameter to engineer these materials [19]. To date, experiments have explored the role of contact friction by examining the effect of changes in particle surface properties on the global response of these systems [11–15]. Yet, these studies have been limited to macroscopic measurements due to the lack of particle-level access to local frictional effects. Consequently, it remains unclear as to how such frictional effects arise due to the microscopic interactions between particles.

In this Letter, we quantitatively relate local coordination to particle-level frictional arrest in an attractive colloidal model system. We reveal that intermittent frictional contacts between pairs of neighbouring particles give rise to an exponential slowdown of the orientational

dynamics of a particle with increasing coordination number. Importantly, our results show that the amount of interparticle friction between pairs of bonded particles can be controllably tuned by varying the strength of the attractive interactions. This is a key step towards using frictional interactions in engineering the properties of colloidal materials.

In our experiments, we use recently developed colloidal particles [20, 21], known as OCULI particles [20], which have a uniform composition and a non-uniform fluorescence profile [Fig. 1(a)]. In particular, these OCULI particles feature an off-centre core, labelled with a complementary fluorescent marker, and a non-fluorescent outer layer that enables the simultaneous tracking of both the centroid positions *and the orientations* of all spheres in three dimensions. Crucially, this provides unprecedented access to frictional interactions between individual particles [20] as the particles' orientations rapidly randomise without interparticle contact, whilst the orientational relaxation is significantly slowed down upon making frictional contact. Note that with 'frictional contact' we mean any type of interaction that constraints rotational motion due to friction, which can arise from solid friction [8, 11], but may also be hydrodynamic in nature [22, 23].

We synthesize OCULI particles of diameter $\sigma = 3.0\mu\text{m}$ (see Methods) following procedures detailed in Ref. [20]. A short-ranged attractive interactions is introduced between the particles by adding non-adsorbing polystyrene polymers (estimated radius of gyration $R_g \approx 105\text{nm}$ [24], see Methods), where the strength of the attractive interactions is varied via the polymer concentration c_p [25, 26]. The attractive OCULI particles are suspended in a density- and refractive index-matching organic solvent mixture and imaged using 3D confocal microscopy (see Methods). Typical images of the resulting colloidal gel are shown in Fig. 1(a1, a2) for different length scales, and a 3D reconstruction of the imaged volume is shown in Fig. 1(b). These colloidal gels, which are comprised of colloidal particles aggregated into a space-spanning network structure [27–29], feature rich structural heterogeneity [30, 31], making them an ideal system to investigate the relation between local structure and frictional effects at the particle level in colloidal matter.

To investigate the emergence of interparticle friction,

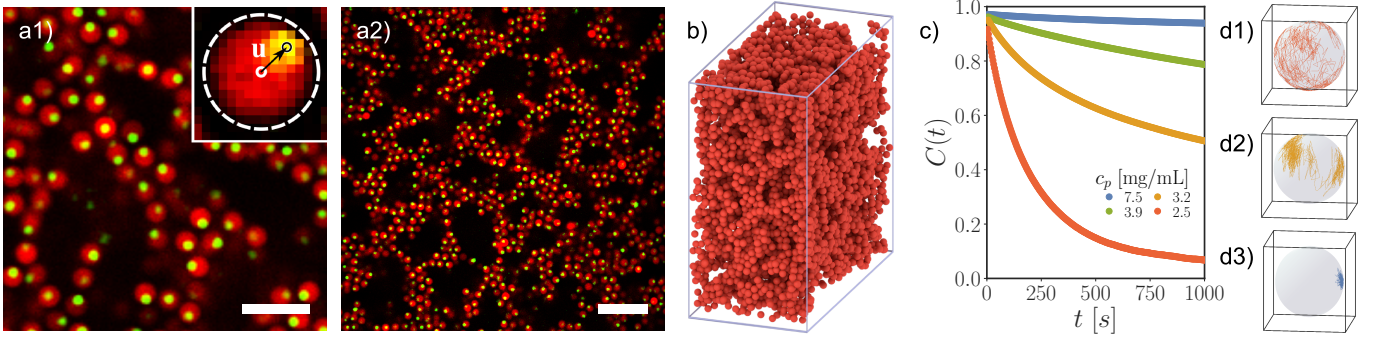


FIG. 1. Orientational dynamics of particles in colloidal gels. (a1, a2) Confocal microscopy images of a colloidal gel of OCULI particles at a polymer concentration $c_p = 3.2$ mg/mL. For each particle the centroids of the red "body" and green/yellow "core" are located to determine its 3D orientation vector \mathbf{u} (see inset in (a1)). Scale bar: (a1) $10 \mu\text{m}$ and (a2) $20 \mu\text{m}$. (b) A 3D rendering of all particles within a typical imaging volume of $102 \times 102 \times 50 \mu\text{m}^3$. (c) Orientational auto-correlation function $C(t)$ for different polymer concentrations c_p . (d1-d3) Typical trajectories of the particle orientation on the unit sphere for polymer concentrations of 2.5, 3.2, and 7.5 mg/mL (top to bottom).

we monitor the orientational dynamics of the particles using the orientational auto-correlation function

$$C(t) = \langle \mathbf{u}_i(t) \cdot \mathbf{u}_i(0) \rangle \quad (1)$$

with $\mathbf{u}_i(t)$ the unit orientation vector of particle i and $\langle \cdot \rangle$ denoting an ensemble-average over all particles. As shown in Fig. 1(c), for weak attractive interactions $C(t)$ rapidly decays indicating a fast randomisation of the particle orientation. For stronger attractive interactions, this orientational relaxation is strongly slowed down or even arrested, giving rise to a clear plateau in $C(t)$. This mobile-to-arrested transition of the orientational dynamics is further illustrated by plotting a typical trajectory of the particle orientation on the unit sphere: at low polymer concentration the particle orientation undergoes constant Brownian rotation [Fig. 1(d1)], while at higher polymer concentration this motion becomes intermittent [Fig. 1(d2)] and eventually fully arrested [Fig. 1(d3)]. We attribute this slowdown of the rotational dynamics to the emergence of *attraction-induced* friction between particles due to interparticle contact. At high attraction strength these contacts are rarely broken by thermal fluctuations, leading to the full arrest of the particle orientation. Our data thus highlight that the emergence of interparticle friction is directly governed by the strength of the attractive interactions. Yet, the ensemble-averaged description provided by $C(t)$ offers no microscopic insight as to how the frictional arrest of a particle arises due to the interaction with neighbouring particles.

To establish a quantitative relation between the local environment of a particle and its frictional arrest, we first quantify the local environment of a particle by its time-averaged coordination number Z_i (see Methods), which is arguably the simplest local structural predictor for orientational arrest. Then, we calculate the orientational autocorrelation function [Eq. 1] again, but now for each

coordination number separately:

$$C(Z, t) = \langle \mathbf{u}_i(t) \cdot \mathbf{u}_i(0) \rangle_Z \quad (2)$$

with Z the coordination number and $\langle \cdot \rangle_Z$ denoting an average over all particles with local coordination $Z_i = Z$. We plot $C(Z, t)$ for a range of attraction strengths in Fig. 2(a1-a4) and observe a clear slowing down of the orientational relaxation with increasing local coordination number, which is especially pronounced at higher attraction strengths [Fig. 2(a1-a3)]. Next, we define the mean orientational relaxation time $\langle \tau_R(Z) \rangle$, which is a measure for the frictional arrest of the orientational dynamics, as follows [32, 33]:

$$\langle \tau_R(Z) \rangle = \int_0^\infty C(Z, t) dt, \quad (3)$$

where in practice we first fit a stretched exponential to $C(Z, t)$ before doing the integration (see Methods). In Fig. 2(b) we plot the mean orientational relaxation time $\langle \tau_R(Z) \rangle$ for different attraction strengths, and $\langle \tau_R(Z) \rangle$ clearly increases exponentially with the local coordination number Z . Interestingly, the slope of the exponential slowdown provides a direct measure for how much the orientational dynamics is slowed down per neighbouring particle, which increases strongly with increasing attraction strength.

To explain the exponential dependence of this coordination-dependent frictional arrest of the orientational dynamics, we start by considering only two attractive particles. Due to thermal fluctuations the pair of particles is subjected to bond-length fluctuations, which we describe using a two-state picture with fluctuations between 'contact' and 'no-contact' states. Here, the 'contact' state leads to arrest of the particle orientation, while the 'no-contact' state allows for relaxation of the particle

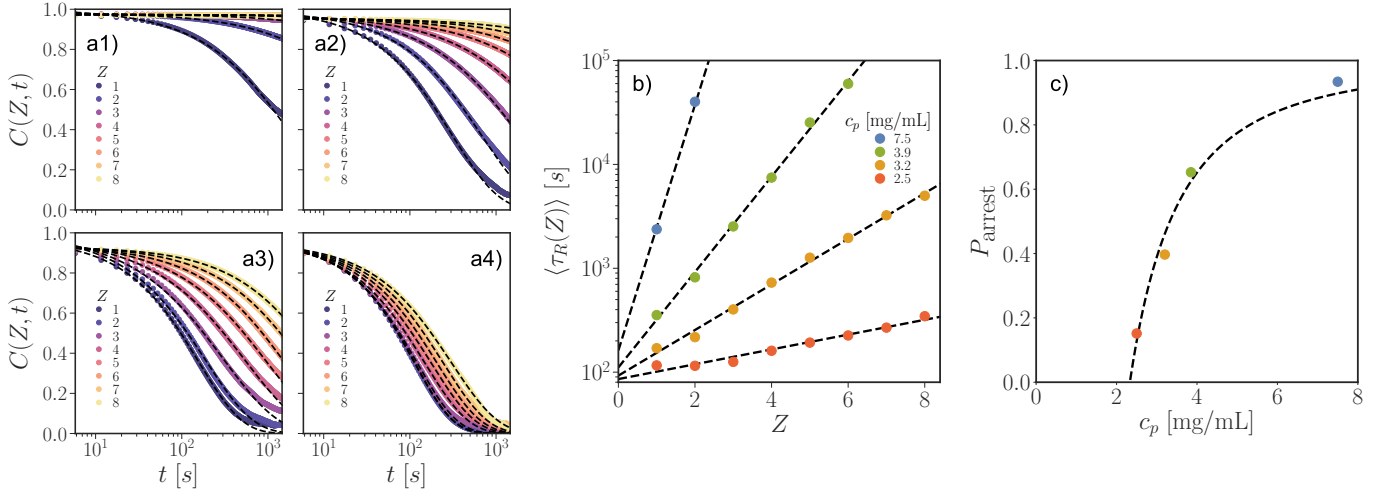


FIG. 2. Coordination-dependent frictional arrest. (a1-a4) The coordination-dependent orientational autocorrelation function $C(Z, t)$ for polymer concentrations $c_p = 7.5, 3.9, 3.2$, and 2.5 mg/mL, respectively. Dashed lines correspond to stretched-exponential fits. (b) The mean orientational relaxation time $\langle \tau_R(Z) \rangle$ as a function of the coordination number Z for different polymer concentrations c_p . Dashed lines are fits to Eq. 5. (c) The probability, i.e. fraction of time, that a pair of neighbouring particles is in the ‘contact’ state P_{arrest} for different polymer concentrations c_p . Dashed line is a guide to the eye.

orientation with a relaxation time τ_0 . As a result, the average orientational relaxation time is simply proportional to the time spent in the ‘no-contact’ state. This can be expressed as

$$\langle \tau_R(Z=1) \rangle \approx \frac{\tau_0}{(1 - P_{\text{arrest}})}, \quad (4)$$

where P_{arrest} is the probability, i.e. fraction of time, that the particle is rotationally arrested due to interparticle friction. Importantly, the above argument for pairs of particles is easily extended to account for larger coordination numbers by assuming that bond fluctuations between all pairs of neighbouring particles are independent of each other, which leads to the following straightforward extension of Eq. 4:

$$\langle \tau_R(Z) \rangle \approx \frac{\tau_0}{(1 - P_{\text{arrest}})^Z}. \quad (5)$$

Here, $(1 - P_{\text{arrest}})^Z$ is thus the probability that all bonds of the central particle with its neighbours are in the ‘no-contact’ state. Crucially, this predicts the experimentally observed exponential increase of the orientational relaxation time with coordination number (see Fig. 2(b)), which thus arises due to the fact that a particle is only able to reorient when it is not in frictional contact with any of its neighbours.

Within our two-state picture the slope of the exponential slowdown is directly related to P_{arrest} , the probability of an interparticle bond being in the ‘contact’ state. To quantify this probability we determine P_{arrest} from our experimental data by fitting the measured relaxation times to Eq. 5 for each attraction strength (dashed lines

in Fig. 2(b)). In Fig. 2(c), we plot P_{arrest} as a function of the polymer concentration and clearly see that interparticle bonds spend increasingly more time in the ‘contact’ state as the strength of the attractive interactions increases. This implies that the attraction strength directly controls the amount of interparticle friction on the level of pairs of particles.

To further establish how the interactions govern the formation of interparticle contacts, we employ a simple computer simulation model which also features the competition between Brownian rotation and friction-induced arrest. To this end, we perform dynamic Monte Carlo computer simulations [34, 35] in which we combine attractive interactions with explicit particle surface roughness (see Methods), which constrains the particle motion via steric interactions. The rough particles are modeled as hard, impenetrable particles to which an attractive depletion interaction is added [Fig. 3(a,b)]. To ensure that sufficiently long time-scales can be explored, the surface roughness is chosen substantially larger than in the experiments. Hence, it is not our goal to directly mimic the experimental situation but much rather to provide a simple model system to test the interplay between attractive interactions and particle-level frictional arrest due to interparticle contacts. As shown in Fig. 3(c), our simple model system captures the behaviour observed in the experiments. Upon plotting $C(Z, t)$ (see SI), we observe a clear dependence of the orientational relaxation of particles on their local coordination with a mean relaxation time $\langle \tau_R(Z) \rangle$ that increases exponentially with particle coordination number Z [Fig. 3(c)]. Furthermore, we also observe that P_{arrest} increases strongly with attraction

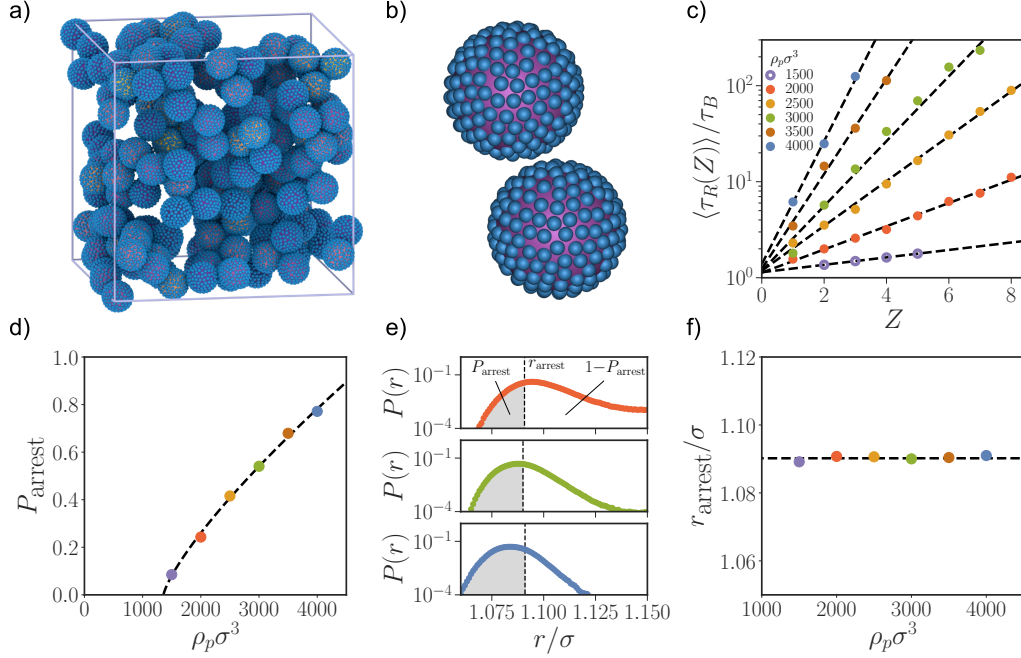


FIG. 3. Dynamic Monte Carlo simulations of attractive particles with explicit surface roughness. (a) Snapshot of a gel at a dimensionless polymer concentration $\rho_p\sigma^3 = 3000$. (b) A close-up of the particles showing clearly the surface topography. (c) The mean orientational relaxation time $\langle\tau_R(Z)\rangle$ as a function of the coordination number Z for different polymer concentrations ρ_p . The relaxation times are rendered dimensionless through normalization with the Brownian time $\tau_B = 1/2D_r$ with D_r the rotational diffusion constant. Solid and open markers correspond to gel and fluid phases, respectively. Dashed lines are fits to Eq. 5. (d) The probability of an interparticle bond being frictionally arrested P_{arrest} as a function of the polymer concentration ρ_p . (e) Probability distribution function of bond lengths $P(r)$ for $\rho_p\sigma^3 = 2000, 3000$ and 4000 (top to bottom). Here r_{arrest} (dashed lines) is determined such that $P(r \leq r_{\text{arrest}}) = P_{\text{arrest}}$ (shaded areas), hence separating the ‘contacting’ and ‘non-contacting’ bond-lengths. (f) Extracted r_{arrest} for different polymer concentrations ρ_p , showing no dependence on the attraction strength.

strength, i.e. interparticle bonding becomes increasingly more frictional [Fig. 3(d)]. The correspondence between the behaviour observed in the simulations and experiments is particularly remarkable considering the large difference in surface roughness of the constituent particles. This underlines the generality of the observed behaviour: the essential physics emerges simply by combining attractive interactions with a constraining ‘contact’ state.

Finally, we reveal that this attraction-induced friction is governed by a length scale associated with the onset of interparticle friction. As it is prohibitively difficult to access such length scale in our experiments due to localization errors and particle polydispersity, we use our simulations to characterize the probability distribution of bond lengths $P(r)$ for a range of attraction strengths by varying the dimensionless polymer concentration $\rho_p\sigma^3$ (see Methods). Clearly, $P(r)$ gets narrower and shifts to shorter bond lengths with increasing attraction strengths [Fig. 3(e)]. The length scale associated with frictional arrest, r_{arrest} , now naturally emerges by separating the bond lengths into ‘contact’ and ‘no-contact’ states via $P(r \leq r_{\text{arrest}}) = P_{\text{arrest}}$ (shaded area in Fig. 3(e)). Interestingly, r_{arrest} is independent of the

attraction strength [Fig. 3(f)], thus revealing the length scale associated with interparticle contact r_{arrest} to be a particle-property, which originates purely from the steric constraints imposed by the surface roughness at bond lengths $r \leq r_{\text{arrest}}$. Our results thus highlight how interparticle frictional interactions can be tuned in colloidal materials: simply by changing the interparticle interactions one can tune the bond-length distribution $P(r)$ to control the fraction of bonds in the ‘contact’ state (shaded area in Fig. 3(e))].

In summary, we have uncovered how local coordination and interparticle interactions govern particle-level frictional arrest in attractive colloidal matter. Our results provide direct and fundamental insight as to how microscopic frictional interactions can be tuned, which provides a novel avenue towards tailoring macroscopic bulk behaviour in these materials. We note that the existence of frictional interactions in particle gels has remained elusive to date due to lack of a direct experimental measurement. Importantly, to date almost all theoretical and simulation studies on such systems do not account for interparticle friction. Incorporating frictional constraints to rolling and sliding between particles

will likely have a pronounced effect on a variety of phenomena studied in attractive colloidal matter such as gel formation, coarsening and failure.

ACKNOWLEDGEMENTS

BvdM acknowledges funding from the Netherlands Organisation for Scientific Research (NWO) through a Rubicon grant (NWO-Rubicon Grant No. 019.191EN.011). RPAD acknowledges the European Research Council (Consolidator Grant No. 724834-OMCIDC). We would like to thank Joanne Verweij and Jeffrey Urbach for useful discussions.

AUTHOR CONTRIBUTIONS

The project was conceived by all authors. BvdM performed particle synthesis. TY provided general expertise and technical assistance with regards to the synthesis, imaging and tracking of the particles. BvdM performed all experiments, computer simulations and data analysis. All authors discussed and interpreted the results. BvdM and RPAD wrote the manuscript with input from TY.

-
- [1] N. Fernandez, R. Mani, D. Rinaldi, D. Kadau, M. Mosquet, H. Lombois-Burger, J. Cayer-Barrioz, H. J. Herrmann, N. D. Spencer, and L. Isa, Microscopic mechanism for shear thickening of non-brownian suspensions, *Physical Review Letters* **111**, 108301 (2013).
 - [2] J. Comtet, G. Chatté, A. Niguès, L. Bocquet, A. Siria, and A. Colin, Pairwise frictional profile between particles determines discontinuous shear thickening transition in non-colloidal suspensions, *Nature Communications* **8**, 1 (2017).
 - [3] R. Seto, R. Mari, J. F. Morris, and M. M. Denn, Discontinuous shear thickening of frictional hard-sphere suspensions, *Physical Review Letters* **111**, 218301 (2013).
 - [4] M. Wyart and M. E. Cates, Discontinuous shear thickening without inertia in dense non-brownian suspensions, *Physical Review Letters* **112**, 098302 (2014).
 - [5] A. Singh, C. Ness, R. Seto, J. J. de Pablo, and H. M. Jaeger, Shear thickening and jamming of dense suspensions: the “roll” of friction, *Physical Review Letters* **124**, 248005 (2020).
 - [6] A. Ikeda, L. Berthier, and P. Sollich, Unified study of glass and jamming rheology in soft particle systems, *Physical Review Letters* **109**, 018301 (2012).
 - [7] R. Mari, R. Seto, J. F. Morris, and M. M. Denn, Discontinuous shear thickening in brownian suspensions by dynamic simulation, *Proceedings of the National Academy of Sciences* **112**, 15326 (2015).
 - [8] B. Guy, M. Hermes, and W. C. K. Poon, Towards a unified description of the rheology of hard-particle suspensions, *Physical Review Letters* **115**, 088304 (2015).
 - [9] J. R. Royer, D. L. Blair, and S. D. Hudson, Rheological signature of frictional interactions in shear thickening suspensions, *Physical Review Letters* **116**, 188301 (2016).
 - [10] N. M. James, E. Han, R. A. L. de la Cruz, J. Jureller, and H. M. Jaeger, Interparticle hydrogen bonding can elicit shear jamming in dense suspensions, *Nature Materials* **17**, 965 (2018).
 - [11] N. Y. Lin, B. M. Guy, M. Hermes, C. Ness, J. Sun, W. C. K. Poon, and I. Cohen, Hydrodynamic and contact contributions to continuous shear thickening in colloidal suspensions, *Physical Review Letters* **115**, 228304 (2015).
 - [12] L. C. Hsiao, S. Jamali, E. Glynos, P. F. Green, R. G. Larson, and M. J. Solomon, Rheological state diagrams for rough colloids in shear flow, *Physical Review Letters* **119**, 158001 (2017).
 - [13] C.-P. Hsu, S. N. Ramakrishna, M. Zanini, N. D. Spencer, and L. Isa, Roughness-dependent tribology effects on discontinuous shear thickening, *Proceedings of the National Academy of Sciences* **115**, 5117 (2018).
 - [14] C.-P. Hsu, J. Mandal, S. N. Ramakrishna, N. D. Spencer, and L. Isa, Exploring the roles of roughness, friction and adhesion in discontinuous shear thickening by means of thermo-responsive particles, *Nature Communications* **12**, 1 (2021).
 - [15] B. Schroyen, C.-P. Hsu, L. Isa, P. Van Puyvelde, and J. Vermant, Stress contributions in colloidal suspensions: The smooth, the rough, and the hairy, *Physical Review Letters* **122**, 218001 (2019).
 - [16] N. Park, V. Rathee, D. L. Blair, and J. C. Conrad, Contact networks enhance shear thickening in attractive colloid-polymer mixtures, *Physical Review Letters* **122**, 228003 (2019).
 - [17] S. Pradeep, M. Nabizadeh, A. R. Jacob, S. Jamali, and L. C. Hsiao, Jamming distance dictates colloidal shear thickening, *Physical Review Letters* **127**, 158002 (2021).
 - [18] B. Ilhan, F. Mugele, and M. H. Duits, Roughness induced rotational slowdown near the colloidal glass transition, *Journal of Colloid and Interface Science* **607**, 1709 (2022).
 - [19] M. Hu, C.-P. Hsu, and L. Isa, Particle surface roughness as a design tool for colloidal systems, *Langmuir* **36**, 11171 (2020).
 - [20] T. Yanagishima, Y. Liu, H. Tanaka, and R. P. A. Dullens, Particle-level visualization of hydrodynamic and frictional couplings in dense suspensions of spherical colloids, *Physical Review X* **11**, 021056 (2021).
 - [21] M. Kamp, B. de Nijs, J. J. Baumberg, and O. A. Scherman, Contact angle as a powerful tool in anisotropic colloid synthesis, *Journal of Colloid and Interface Science* **581**, 417 (2021).
 - [22] S. Jamali and J. F. Brady, Alternative frictional model for discontinuous shear thickening of dense suspensions: Hydrodynamics, *Physical Review Letters* **123**, 138002 (2019).
 - [23] M. Wang, S. Jamali, and J. F. Brady, A hydrodynamic model for discontinuous shear-thickening in dense suspensions, *Journal of Rheology* **64**, 379 (2020).
 - [24] B. Vincent, The calculation of depletion layer thickness as a function of bulk polymer concentration, *Colloids and Surfaces* **50**, 241 (1990).
 - [25] S. Asakura and F. Oosawa, On interaction between two bodies immersed in a solution of macromolecules, *The Journal of Chemical Physics* **22**, 1255 (1954).

- [26] S. Asakura and F. Oosawa, Interaction between particles suspended in solutions of macromolecules, *Journal of Polymer Science* **33**, 183 (1958).
- [27] A. D. Dinsmore and D. A. Weitz, Direct imaging of three-dimensional structure and topology of colloidal gels, *Journal of Physics: Condensed Matter* **14**, 7581 (2002).
- [28] A. D. Dinsmore, V. Prasad, I. Wong, and D. A. Weitz, Microscopic structure and elasticity of weakly aggregated colloidal gels, *Physical Review Letters* **96**, 185502 (2006).
- [29] P. J. Lu, E. Zaccarelli, F. Ciulla, A. B. Schofield, F. Sciortino, and D. A. Weitz, Gelation of particles with short-range attraction, *Nature* **453**, 499 (2008).
- [30] J. M. van Doorn, J. Bronkhorst, R. Higler, T. van de Laar, and J. Sprakel, Linking particle dynamics to local connectivity in colloidal gels, *Physical Review Letters* **118**, 188001 (2017).
- [31] K. A. Whitaker, Z. Varga, L. C. Hsiao, M. J. Solomon, J. W. Swan, and E. M. Furst, Colloidal gel elasticity arises from the packing of locally glassy clusters, *Nature Communications* **10**, 1 (2019).
- [32] C. P. Lindsey and G. D. Patterson, Detailed comparison of the williams–watts and cole–davidson functions, *The Journal of Chemical Physics* **73**, 3348 (1980).
- [33] F. Alvarez, A. Alegria, and J. Colmenero, Relationship between the time-domain kohrausch-williams-watts and frequency-domain havriliak-negami relaxation functions, *Physical Review B* **44**, 7306 (1991).
- [34] E. Sanz and D. Marenduzzo, Dynamic monte carlo versus brownian dynamics: A comparison for self-diffusion and crystallization in colloidal fluids, *The Journal of Chemical Physics* **132**, 194102 (2010).
- [35] F. Romano, C. De Michele, D. Marenduzzo, and E. Sanz, Monte carlo and event-driven dynamics of brownian particles with orientational degrees of freedom, *The Journal of Chemical Physics* **135**, 124106 (2011).

METHODS

Experimental details

Colloidal particles

We synthesize 3-trimethoxysilyl propyl methacrylate (TPM) OCULI particles, which are coated with a non-fluorescent outer layer, following the four-stage synthesis described in detail in Ref. [20]. In short, monodisperse droplets were created by mixing a pre-hydrolysed TPM solution with a basic solution. These droplets were labelled with green fluorescent BDP-FL dye and subsequently cross-linked, resulting in TPM core particles. Subsequently, these core particles were used to create OCULI particles via seeded emulsion polymerization. Here, each core particle is engulfed by a TPM droplet, which was labelled with red fluorescent Cy3 dye and subsequently cross-linked. In the final two steps, an additional non-fluorescent outer layer of TPM was grown around the particles. This ensures a proper separation between fluorescent signals of different particles, which allows us to track all particles positions and orientations in 3D – even when particles are in direct contact. To this end, the OCULI particles were covered with small TPM lobes, resulting in “raspberry”-shaped OCULI. In the final synthesis stage, the space between the lobes were filled with a final layer of TPM to create a smooth, spherical particles. Importantly, as the particles are fully made of TPM we can density- and index-matched these particles in a organic solvent mixture, allowing us to image deep inside dense materials and minimize gravitational stresses.

The particles were characterized using both Scanning Electron Microscopy (SEM) and confocal microscopy (see SI). Sizing the particles using SEM yielded a diameter $\sigma_{\text{SEM}} = 2.78 \mu\text{m}$ with a polydispersity of 3.1%. In our confocal microscopy experiments, these particles are slightly larger in diameter compared to the SEM-measurements due to swelling in the organic solvent mixture [20]. Using confocal microscopy experiments in which we measured the translational and rotational diffusivity of a dilute suspension of particles, we determined the particles to have a final diameter of $\sigma = 3.0 \mu\text{m}$ in the organic solvent mixture.

Attractive interactions

We introduce a short-ranged attractive interaction between the particles by adding non-adsorbing polystyrene polymers. The polystyrene polymer was obtained from Agilent Technologies and has a molar weight $M_w = 1.23 \times 10^7 \text{ g/mol}$ and polydispersity $M_w/M_n = 1.19$. Following Ref. [24], the radius of gyration of the polymer at

theta-solvent conditions is estimated to be $R_g \approx 105\text{nm}$. In our experiments, however, the organic solvent mixture may act as a good solvent for the polystyrene polymers, which would lead to an increase in polymer size due to swelling.

Sample preparation and confocal microscopy

In our experiments, we carefully density- and index-matched our particles using a ternary solvent mixture of tetralin, trichloroethylene and tetrachloroethylene containing 5wt% OLOA 11000. Using this organic solvent mixture, we prepared separate stock solutions of the colloids and the polymer, which were allowed to equilibrate for several days. Colloid-polymer mixtures with a colloid volume fraction of $\phi \approx 0.3$ and desired polymer concentration were created by combining the stock solutions into a vial. The mixture was vortex-mixed to ensure proper homogenisation and loaded into a rectangular capillary (0.10 x 2.00 mm, VitroCom) which was subsequently sealed using epoxy glue. The sample was rotated slowly for an hour on a mini-rotator to allow the formation of a colloidal gel (see SI for characterization) while any residual gravitational stresses are minimized.

The colloidal gels were imaged using 3D confocal laser-scanning microscopy. The confocal microscope consists of an Olympus IX73 inverted microscope with an 60x Olympus Plan Apochromat oil immersion objective (NA = 1.42). High-speed 3D imaging is achieved using a Thorlabs confocal 12kHz resonant scanner and an objective-mounted piezoelectric Z-stage (Physik Instrumente). Using 488-nm and 532-nm lasers for excitation, a two-channel imaging volume of $102 \times 102 \times 50\mu\text{m}^3$ was recorded at intervals of 5.81s over 800 stacks. The particles' coordinates and orientations were determined using the locating algorithm detailed in Ref. [20].

Analysis details

Local coordination

To track the time-dependent local coordination $Z_i(t)$ of a particle i , we determine the number of neighboring particles located within a cutoff distance r_c . In the experiments, two particles are considered to be neighbours when their centres are separated by a distance $r_c \leq 3.6\mu\text{m}$, which is chosen slightly larger than the range of the depletion interaction ($\sigma + 2R_g \approx 3.3\mu\text{m}$) to account for polydispersity and localization errors. This choice of r_c corresponds roughly to the first minimum in the radial distribution function. Furthermore, we have checked that our results are robust to variations in r_c . In the simulations, particles are considered to be neighbours if their

centres are within the attractive range of the depletion interaction $r_c \leq \sigma + \sigma_p$.

Due to thermal fluctuations the local coordination number of a particle is slightly fluctuating in time. Hence, for the calculation of the coordination-dependent orientational autocorrelation function $C(Z, t)$ we time-averaged the particle's coordination number over the delay time t and subsequently rounded it to the nearest integer.

Mean orientational relaxation time

Following Refs. [32, 33], we define the mean orientational relaxation time $\langle \tau_R(Z) \rangle$ as the area under the curve $C(Z, t)$ [Eq. 3]. In practise, directly integrating the measured $C(Z, t)$ is not possible as they do not always fully decay within the observation time. To this end, prior to integration, we first fitted each $C(Z, t)$ to the Kohlrausch-Williams-Watts stretched exponential function (dashed lines in Fig. 2(b1-b3)):

$$C(Z, t) = (1 - \epsilon^2) \exp[-(t/\tau)^\beta], \quad (6)$$

where τ is the time constant, β the exponent, and ϵ captures both the measurement error in the particle orientation and fluctuations at larger length scales due to internal flexibility within the gel structure.

Simulation details

Preparation of particles with explicit surface roughness

A particle with a rough surface was generated by covering the surface of a spherical base particle of diameter σ with $N_s = 200$ small asperities of diameter $\sigma_s = 0.118\sigma$. Here, the centre-to-centre distance between the large and small spheres was fixed to the large-particle radius. Initially, the small-spheres were assigned a random position on the large-particle surface and many overlaps between small spheres resulted. To obtain an even coverage, a short Monte Carlo simulation was performed in which small-sphere asperities interact with each other as hard spheres. A particle configuration free from small-sphere overlaps was obtained, after which the simulation was stopped after an additional 10^4 MC sweeps. This particle configuration was used in all dynamic Monte Carlo simulations.

Dynamic Monte Carlo simulations

We perform dynamic Monte Carlo simulations [34, 35] of $N = 216$ rough particles in the NVT -ensemble. These

particles are modelled as hard particles with an additional attractive depletion interaction:

$$\beta U_{tot}(\mathbf{r}_{ij}, \hat{\omega}_i, \hat{\omega}_j) = \beta U_{hc}(\mathbf{r}_{ij}, \hat{\omega}_i, \hat{\omega}_j) + \beta U_{attr}(r_{ij}), \quad (7)$$

where \mathbf{r}_{ij} is the center-to-center separation vector between two particles i and j , $\hat{\omega}_i$ the orientation of particle i , and $U_{hc}(\mathbf{r}_{ij}, \hat{\omega}_i, \hat{\omega}_j)$ is the orientation-dependent hard-core interaction potential, which is infinite when the particles overlap and zero otherwise. Attractive interactions are introduced using the Asakura-Oosawa depletion model [25, 26]:

$$\beta U_{attr}(r_{ij}) = \begin{cases} -\frac{\pi\sigma_p^3\rho_p}{6} \frac{(1+q)^3}{q^3} \\ \times \left[1 - \frac{3r_{ij}}{2(1+q)\sigma} + \frac{r_{ij}^3}{2(1+q)^3\sigma^3} \right], & \text{for } \sigma < r_{ij} < \sigma + \sigma_p \\ 0, & \text{otherwise} \end{cases} \quad (8)$$

where σ_p is the polymer diameter and $q = \sigma_p/\sigma = 0.15$ is the polymer-colloid size ratio which controls the range of the attractive interaction. The strength of the attractive interaction depends linearly on the polymer reservoir density ρ_p , i.e. the number density of ideal polymers in a reservoir that is in chemical equilibrium with the colloid-polymer mixture. Note that in order to keep our model as simple as possible, we have chosen not to account for surface-roughness effects on the depletion interactions.

As the dynamic Monte Carlo method requires the system to be evolved via small moves with a high acceptance

ratio [34, 35], we first perform a regular Monte Carlo simulation in which particles are displaced and rotated in larger steps in order to efficiently create a starting configuration for our dynamic Monte Carlo simulations. To this end, we start off by simulating a fluid of purely repulsive rough particles ($\rho_p\sigma^3 = 0$) at a fixed particle number density $\rho = N/V = 0.38$. After a short simulation time of 10^5 MC cycles, the attractive interactions are switched on and the system is evolved for 10^6 MC cycles. At sufficiently high attraction strength ($\rho_p\sigma^3 \gtrsim 2000$) this results into the formation of a particle gel, whereas at lower attraction strengths a fluid phase forms.

Starting from these configurations, we investigate the dynamics of the attractive rough particle system using the dynamic Monte Carlo method [34, 35], which evolves the system via small translational and rotational MC moves at a high acceptance rate. Here, a particle was translated by displacing it a random amount in the interval $[-\delta_t, \delta_t]$ for each cartesian axis. Likewise, a particle was rotated by rotating it a random amount in the interval $[0, \delta_r]$ around a randomly chosen axis. Importantly, following the iterative procedure in Ref. [35] we carefully set δ_t and δ_r to match the diffusivity of the orientational and translational degrees of freedom such that particles diffuse according to the Stokes–Einstein equation. Here, δ_t and δ_r are chosen to be small to achieve a high acceptance ratio (> 0.8). This ensures that the Monte Carlo dynamics can be mapped unto an accurate Brownian dynamics for particles with orientational degrees of freedom [35].